LBNL-39178
UC-404

ERNEST ORLANDO LAWRENCE
BERKELEY NATIONAL LABORATORY

The Influence of Microstructure on the Mechanical Properties of Solder

J.W. Morris, Jr. and H.L. Reynolds
Materials Sciences Division
Center for Advanced Materials

June 1996
Presented at the
SEM (Society for Experimental Mechanics) Conference,
Nashville, TN,
June 10-13, 1996,
and to be published in
the Proceedings

LBL-39178

THE INFLUENCE OF MICROSTRUCTURE ON THE MECHANICAL PROPERTIES OF SOLDER

J. W. Morris Jr., and H.L. Reynolds

Department of Materials Science and Mineral Engineering
University of California, Berkeley

and

Center for Advanced Materials
Materials Sciences Division
Lawrence Berkeley National Laboratory
Berkeley, CA 94720

June 1996

This work is supported by the Director, Office of Energy Research, Office of Basic Energy Science, Material Sciences Division of the U.S. Department of Energy under Contract No. DE-AC03-76SF00098

THE INFLUENCE OF MICROSTRUCTURE ON THE MECHANICAL PROPERTIES OF SOLDER

J.W. Morris, Jr., and H. L. Reynolds
Department of Materials Science, University of California, Berkeley, and
Center for Advanced Materials, Lawrence Berkeley Laboratory

Solder joints in microelectronics devices consist of low-melting solder compositions that wet and join metal contacts and are, ordinarily, used at high homologous temperatures in the as-solidified condition. Differences in solidification rate and substrate interactions have the consequence that even solder joints of similar compositions exhibit a wide range of microstructures. The variation in microstructure causes a variation in properties; in particular, the high-temperature creep properties that govern much of the mechanical behavior of the solder may differ significantly from joint to joint. The present paper reviews the varieties of microstructure that are found in common solder joints, and describes some of the ways in which microstructural changes affect mechanical properties and joint reliability.

INTRODUCTION

As the microelectronics industry has matured, quality and reliability have become almost as important as performance in defining advanced technology. The metallic conductors that connect the active elements of a microelectronic device are critical to its reliability. The small size and severe operating environment of these interconnects makes them liable to unusual metallurgical failure modes that must be understood and controlled to guarantee reliable performance. Because of their unique features, these failure modes are scientifically interesting as well as technologically important.

There are three common mechanical failure modes that occur in modern solder joints: fracture during handling, which is governed by the ultimate tensile strength, thermal fatigue during service, which is governed by the fatigue resistance, and, particularly in optoelectronic devices, dimensional changes, which are often the result of stress and stress relaxation. To predict and control these failure modes one needs to understand the mechanical properties of the solder. As is the case with all material properties, these are jointly determined by the composition of the solder (what chemical species it contains) and its microstructure (how those species are physically distributed through the solder joint).

The notion that the properties of a solder joint are influenced by its chemical composition is well known to virtually all engineers who are interested in the subject. However, the importance of the microstructure of the joint is not so widely appreciated by those who are not specialists in mechanical metallurgy. It is common to find published compilations of the properties of solder compositions or reports on the behavior of solder joints that make no reference to the microstructure at all. Since important mechanical properties, such as the creep rates of common solder compositions, can vary by orders of magnitude as the microstructure is changed, the failure to appreciate the role of microstructure can lead to serious errors in the design of solder joints or the prediction of lifetime in service.

On the other hand, it is a historical fact that the neglect of solder microstructure has not caused the widespread problems that a metallurgist might intuitively expect. There are at least two reasons for this. First, solder joints are ordinarily used in the as-solidified condition, with the consequence that their microstructures are primarily determined by the rate of solidification, which depends largely on the physical size of the joint. It follows that chemically and geometrically similar solder joints tend to have similar microstructures, and, hence, similar behavior. Design experience with a particular type of joint, which may be codified in empirical rules governing strength and fatigue life, can often be transferred from one device to another with no serious risk. Since the vast majority of solder joints employ one of only a few compositions and interface metallurgies (for example, eutectic Pb-Sn on Cu), prior experience is often a reliable guide. Second, the mechanical property data that is used to guide joint design is commonly taken from bulk solder specimens that are solidified relatively slowly. These tend to have a significantly lower strain-to-failure and a much shorter thermal fatigue life than the most rapidly cooled solder joints that are actually used in devices. As a consequence, there is often an inherent added margin of safety in the data that is used to guide joint design.

At least two trends in the design of joints for modern electronic devices are eroding the historical margin-of-safety, and making it more important that designers consider the specific microstructures of the solders they use. The first trend is the increasing use of new solder compositions that are specifically tailored for particular devices and manufacturing processes. Examples include the low-melting compositions that are employed to reduce thermal damage to sensitive components, particularly in optoelectronic devices, and the Pb-free compositions that have been adopted to meet environmental concerns. These new compositions do not have the empirical base of the Pb-Sn solders, and cannot automatically be assumed to have the same built-in margins of safety in the translation from bulk to joint behavior. The second trend is the miniaturization of microelectronics packaging, which often requires that joints be used under stringent conditions with smaller margins of safety. If the designer cannot simply boost the size of a joint to ensure its reliability, he must have an accurate representation of its mechanical behavior.

In the following we shall briefly describe the microstructures of typical solder joints, and discuss the influence of microstructure on mechanical behavior. The

mechanical behavior of greatest interest is high-temperature creep. Since solder joints are used at temperatures close to their melting points, their deformation under load is governed by creep, which ordinarily determines tensile strength in shear, stress relaxation, and thermal fatigue.

THE MICROSTRUCTURES OF TYPICAL SOLDER JOINTS

The most common solder joints employ Sn-bearing solders (Sn-Pb, Sn-In, Sn-Bi, Sn-Ag, or ternaries of these) that join contacts made of Cu or Ni, which may be coated with Au. The solder joint is, hence, a sandwich composite in which plates of relatively hard metal (Cu or Ni) bound a relatively soft body of solder. The metal-solder interface is generally coated with an intermetallic layer that is formed by reaction between the substrate material and species in the solder. Sn and In react with Cu and Au, Sn reacts with Ni. The final microstructure is determined by the solidification behavior of the solder and the reaction at the solder-metal interface. If the solder is used at a high homologous temperature, as it ordinarily is, the microstructure may evolve during service.

The microstructure of bulk solder

We have previously reviewed the microstructures of bulk solders in some detail [1-3]. Most of the important solder microstructures are exhibited by the Pb-Sn system, which provides the most widely used solder compositions.

The simple eutectic phase diagram of the Pb-Sn system is drawn in Fig. 1, and provides a good reference for the purposes of discussion. The microstructures that result from solidification in a simple eutectic system depend on the composition and cooling rate. The three prototype cases are indicated in the figure: eutectic (labeled (1) in the figure), off-eutectic (labeled (2)), and solvent-rich (labeled (3)).

Eutectic microstructures

If a material with a eutectic composition (labeled (1) in Fig. 1) is solidified by cooling relatively slowly it forms the classic "eutectic" microstructure shown in Fig. 2. The two solid solutions that make up the eutectic grow simultaneously and parallel to one another in grain-like colonies like those shown in the figure. If the two phases are present in roughly equal volume fraction, they grow as parallel plates within each colony. If one phase predominates, the second ordinarily forms discrete rods in the matrix of the other.

The microstructure of eutectic material changes with the rate of solidification. Figure 3, which is taken from ref. [4], compares the microstructures of eutectic Pb-Sn at three cooling rates. Slow cooling during solidification produces a classic eutectic microstructure (Fig. 3a). Very rapid cooling leads to a quite different microstructure in which the Pb-rich and Sn-rich phases form small, almost equiaxed grains that are intermixed with one another (Fig. 3c). Intermediate cooling rates produce

microstructures that lie between these two extremes. It is important to note that all three microstructures are observed in solder joints in electronic devices. The relatively massive joints that are made, for example, on printed wiring boards or at the boundaries of ceramic chip carriers tend to have eutectic microstructures like that shown in Fig. 3a, while the much smaller joints that are used in many surface-mount structures have microstructures that resemble those in Fig. 3b or 3c.

The eutectic microstructure can also be modified by chemical additives. When a third chemical species is present in significant concentration, it changes the phase diagram, and may alter the microstructure for this reason. But additives can also affect the microstructure by changing the kinetics of solidification, even when their concentrations are small. In some cases these additives are made intentionally. For example, we showed some years ago [5,6] that small additions of In or Cd would perturb the growth of the eutectic microstructure of Pb-Sn, presumably because these species are rejected into the eutectic colony boundaries during growth. Fig. 4 illustrates the effect of In on eutectic Pb-Sn. In other cases the ternary chemical addition is inadvertent. For example, species may dissolve into the solder from the substrate. Fig. 5 compares the microstructures of eutectic In-Sn solder after solidification at comparable rates on Cu and Ni substrates [7]. A small amount of Cu dissolves into the solder, while Ni does not. The result is that In-Sn develops a well-defined eutectic microstructure on the Ni substrate, but has an irregular, less defined microstructure when bonding Cu.

Evolution of eutectic material during service

As is the case with any metal casting, the as-solidified microstructure of solder is a non-equilibrium structure. But solder differs from the common structural metal castings in that it is used at high homologous temperatures where solid state diffusion can occur at an appreciable rate. As a consequence the microstructure of the solder may change during service, along a path that takes it to a more nearly equilibrium state. The as-solidified microstructure of a typical eutectic solder is out of equilibrium in three respects, which lead to three distinct kinds of microstructural equilibrium during service.

First, as-solidified eutectic material is usually out of equilibrium in the compositions and volume fractions of its constituent phases. The reason is obvious from the phase diagram shown in Fig. 1, which represents the Pb-Sn system, but is reasonably typical of the other common eutectics. When material with the eutectic composition (labeled 1 in the figure) is cooled from the liquid phase, it solidifies at the eutectic temperature into a mixture of terminal solid solutions that have compositions given by the terminal points of the eutectic line. As the temperature is lowered below the eutectic, the equilibrium solute content of the terminal solutions decreases. This decrease may be significant, as is, for example, the solubility of Sn in Pb according to the phase diagram in Fig. 1. Since solid-state diffusion is relatively slow, the supersaturation is ordinarily relieved by precipitation within the solute-rich grains. Hence the Pb-rich phase in eutectic Pb-Sn is ordinarily decorated with fine precipitates of Sn. In Bi-Sn, the solubility of Bi in the Sn-rich phase is strongly temperature-dependent, so this phase becomes decorated with Bi precipitates, as illustrated in Fig. 6. This phenomenon has the

effect of strengthening the decorated phase. More importantly, in optoelectronic and other applications where dimensional tolerances are very tight, the changes in composition and phase fraction can change the volume of the solder, which may cause misalignment.

Second, as-solidified eutectic material is out of equilibrium with respect to changes that decrease the interfacial area per unit volume. The interfacial area per unit volume is particularly high in the eutectic microstructure because of the plate- or rod-shaped grains. There are two mechanisms available to relieve the excess surface energy. The first is the gradual coarsening and spheroidization of the lamellae within the eutectic colonies. This process usually initiates at the colony boundaries, where the eutectic structure is disturbed in any case, and works its way inward. It occurs gradually in all eutectic microstructures, at a rate that increases with the homologous temperature, and may also be accelerated by solute species that accumulate at interfaces, such as Pb in Bi-Sn. A more striking microstructural change intrudes when a eutectic microstructure is plastically deformed at a high homologous temperature. In this case the solder may spontaneously recrystallize into fine, equiaxed grains. This process is particularly likely in Pb-Sn and Bi-Sn eutectics deformed in shear [7,8,9,13]. The recrystallization concentrates along bands of inhomogeneous shear, as illustrated in Fig. 7. The development of this type of inhomogeneous microstructure can lead to a dramatic deterioration in fatigue strength.

Rapidly solidified material also has a high surface area because of its fine initial grain size. While fine-grained, equiaxed material does not ordinarily recrystallize under load, the grains do grow monotonically, causing a change in those mechanical properties that are influenced by fine grain size.

Third, a solder joint is out of equilibrium with respect to the gradual growth of reactant phases at the solder-substrate interface. Particularly in the case of Sn-containing solders on Cu, the gradual growth of Cu-Sn intermetallics at the interface is accompanied by the depletion of Sn from the material adjacent to the interface, producing a Pb-rich band along the interface, as illustrated in Fig. 8. [31]

Off-eutectic microstructures

The vertical line labeled (2) in Fig. 1 is drawn at an off-eutectic composition. When an off-eutectic solder of this composition is solidified by cooling at a slow to moderate rate, the α-phase forms as discrete islands at temperatures within the α+L field. In the simplest case, the as-solidified microstructure resembles that shown in Fig. 9 [15]; islands of pro-eutectic constituent are distributed through a matrix that has a classic eutectic microstructure.

Because the starting composition is not quite right for the classic eutectic microstructure, it is often possible to solidify an off-eutectic solder into a fine-grained, equiaxed microstructure at low to moderate cooling rates. this is particularly true when the solder contains three or more species that must be redistributed. Fig. 10, for example,

shows the fine-grained as-solidified structure of a 40In40Sn20Pb solder joint that was solidified at a moderate cooling rate [10].

Precipitated microstructures

A composition like that labeled (3) in Fig. 1 solidifies into a polygranular microstructure of a single phase (α in the example given in the figure). On further cooling, the solder penetrates the two-phase ($\alpha+\beta$) region, and β-phase precipitates within the matrix of α. 95Pb-5Sn is a widely used solder that has this solidification behavior.

When a precipitated microstructure is aged at a relatively high homologous temperature, both the grains and the precipitates gradually grow. Both the rate and pattern of growth may be more dramatic if the material is thermally cycled. If the composition and temperature change are such that the thermal cycle penetrates the single-phase region (the α region in Fig. 1), the precipitates dissolve and re-form during each cycle. This can lead to accelerated growth, or to the reconfiguration of the precipitate phase into grain boundaries or regions of high internal stress.

Similar instabilities are observed if the material is stressed at high temperature. If the solute-rich precipitate causes a volume or shape change when it forms, then a reconfiguration of the precipitate distribution causes a mechanical strain. At high temperature solute diffusion is relatively rapid, and the precipitate distribution may change in a way that serves to relax the imposed stress.

Intermetallic reactions at the solder-substrate interface

The solder is intended to wet the metal surfaces it joins and form a strong bond between them. Both wetting and bonding are enhanced if there is a chemical reaction between the solder and the substrate. The most common interfacial reaction is between Sn in the solder and Cu or Ni in the substrate to form Sn-rich intermetallics. Indium also forms intermetallics with Cu and Au.

The most common intermetallics are the two Cu-Sn compounds, Cu_3Sn, and Cu_6Sn_5. Cu_3Sn forms when there is an excess of Cu; for example, it is often found at interfaces between Cu and Pb-rich solders such as 95Pb-5Sn. Cu_6Sn_5 forms preferentially in excess Sn, and is, therefore, the usual interfacial intermetallic in eutectic Pb-Sn solder joints (63Sn-37Pb) and at Cu-Sn interfaces. In this case, however, the intermetallic layer is usually a composite, with Cu_3Sn at the copper interface (Fig. 11). The relative amounts of the two intermetallics increase with the growth temperature in a predictable way [11].

The morphology of the intermetallic layer reflects the crystal structure of the intermetallic. Cu_3Sn is orthorhombic in structure, and tends to form a tightly coherent layer with nearly equiaxed grains [12]. Cu_6Sn_5 is hexagonal, and tends to form a rough layer with knobs or hexagonal prisms that extend into the solder, as illustrated in Fig. 12 [13].

Intermetallics within the bulk

Intermetallic phases may also appear within the bulk solder. There are two common sources for these intermetallics.

First, intermetallic phases may grow out from the interface into the molten solder, and break off to be trapped in the bulk solder during freezing. Examples include the long, hexagonal rods of Cu_6Sn_5 sometimes found in Pb-Sn solder immediately after solidification [13], and the blocky, In_2Au intermetallics found near the interface when In-rich solders wet Au-coated substrates [3] (Fig.13). Second, intermetallics may precipitate within solder that is supersaturated by the dissolution of material from the substrate. Examples include the formation of a dense distribution of $AuSn_4$ intermetallic particles within Pb-Sn solder on wetting a Au-coated substrate [14] (Fig. 14), and the formation of Cu-Sn intermetallics ahead of the interface during the aging of Cu joints with thin, pre-tinned layers [11] (Fig. 15).

The formation and growth of intermetallic precipitates has a second, indirect influence on the microstructure of the joint; it changes the composition of the solder by depleting it of the constituent that participates in the intermetallic. For example, if eutectic Sn-Pb wets a Au-coated interface the composition of the molten solder shifts to the Pb-rich side of the eutectic value, and the solidified solder contains islands of pro-eutectic Pb as well as Au-Sn intermetallic precipitates (Fig. 14). When the intermetallic (Cu-Sn for example) grows in the solid state, the depletion of Sn creates a Pb-rich layer ahead of the growing intermetallic, and produces a chemically inhomogeneous solder (Fig. 8).

THE INFLUENCE OF MICROSTRUCTURE ON MECHANICAL PROPERTIES

Since the melting points of common solders are only slightly above room temperature, they deform in high-temperature creep, and their mechanical properties and failure modes are those associated with creep, stress relaxation and creep fatigue. A thorough discussion of the influence of microstructure on these properties is beyond the scope of this paper, and has been done, in part, elsewhere[2,3]. In the following we briefly describe a few of the more obvious effects.

The creep rate

Fig. 16 is a standard creep curve [16] that illustrates the variation of plastic strain with time at high temperature under constant load. The creep response is conveniently divided into three regimes, called primary, steady-state, and tertiary creep. During primary creep the strain rate decreases with strain, reaching a steady-state value that is preserved for some period of time, then monotonically increases until the material fails. In most solders, primary creep is not extensive, and the creep behavior at small to moderate strains is well characterized by the steady-state creep rate. In the Dorn picture [17], which we shall adopt here, the steady state creep rate is governed by a microstructurally determined "rate-controlling step", which is thermally activated, and leads to a constitutive equation of the form

$$\dot{\gamma} = A\tau^n \exp[-Q/kT] \qquad (1)$$

where $\dot{\gamma}$ is the shear strain rate, τ is the shear stress, n is the stress exponent, and Q is the activation energy. The stress exponent, n, and the activation energy, Q, change with the dominant creep mechanism, and may have different values in different regimes of the applied stress.

The range of creep mechanisms that is pertinent to the behavior of typical solders is illustrated by the steady-state behavior of fine-grained, eutectic Pb-Sn, which is shown schematically in Fig. 17 [18]. At relatively high stress creep is governed by a stress exponent in the range 4-7, with an activation energy that is close to that for bulk diffusion. Deformation is reasonably homogeneous through the bulk, and the rate-controlling step is believed to be associated with the climb of dislocations in the interior of the grains. At intermediate stresses creep is governed by a stress exponent near 2, with an activation energy near that for grain boundary diffusion (about one-half the bulk value). Deformation is concentrated along grain boundaries, and the rate-controlling mechanism is believed to be grain boundary sliding. At still lower stresses the stress exponent increases to about 3, and the activation energy returns to a value appropriate to bulk diffusion. Deformation is still concentrated near grain boundaries, and the rate-controlling step is believed to be the bulk deformation that is needed to preserve grain contact during grain boundary sliding.

The influence of microstructure on the creep rate of eutectic Pb-Sn is primarily through the grain size (colony size in the case of the classic eutectic microstructure), and is illustrated schematically in Fig. 18. As the grain size increases, the solder hardens, particularly at lower value of the strain rate, and the intermediate creep mechanism disappears. This behavior is, at least qualitatively, common to all eutectic materials. The extent to which it is relevant to a specific solder depends on the ease with which the microstructure varies with the cooling rate during solidification, which is affected, for example, by the size of the solder joint. The behavior shown in Fig. 18 is easily observed in eutectic Pb-Sn [1], since it is relatively easy to change the microstructure from a classic eutectic to a fine-grained, equiaxed mixture by increasing the cooling rate. It is less pertinent to other eutectic solders whose microstructures are relatively insensitive to cooling rate. Eutectic Bi-Sn, for example, preserves a classic eutectic microstructure over a wide range of cooling rates; as shown in Fig. 19, its creep behavior is nearly constant over this range.

The creep rate and mechanism are also affected by chemical changes that alter the microstructure. Fig. 5, above, shows the difference microstructure of eutectic In-Sn on Cu and Ni substrates, which appears to be due to Cu accumulation in the solder. Fig. 20 shows that the creep behavior in the two cases is dramatically different [33]. Fig. 14, above, illustrates how Pb-Sn eutectic solder is densely decorated by Au-Sn intermetallics when it wets a Au-coated substrate. Fig. 21 shows how the creep behavior is altered, particularly in the low-stress region [19].

It is conventional, and generally useful, to use the governing equation for the steady state creep rate as the constitutive equation for the deformation of solder under load. These examples illustrate that the constitutive equation must be determined for the specific microstructure of the solder that is being modeled.

The shear strength at low to moderate strain rate

When a typical material is tested in creep at constant stress, as in Fig. 16, the steady state represents the minimum strain rate. Conversely, when the material is tested at constant strain rate, steady state creep determines the maximum stress and, hence, places an upper limit on the shear strength. It follows that the shear strength of a solder can often be inferred from its steady state creep curve. This result is illustrated in Fig. 22 [20] which plots the results of shear strength tests on Bi-Sn solder joints. The shear strength data lies on a simple extrapolation of the steady state creep curve. Furthermore, it has been suggested by others [26,27] that, to first order, the creep behavior of Pb-Sn eutectic solder along any loading path (tension, relaxation, creep, or fatigue) can be treated with a steady state expression where n is a function of stress.

Microstructural changes that alter the steady-state creep curve also affect the shear strength. For example, increasing the effective grain size increases the shear strength, as illustrated in Fig. 18.

The microstructure also affects the failure strain. The effect is particularly strong in the limiting cases of the fine-grained and the classic eutectic microstructures. A sample that is fine-grained and tested at the strain rates for which grain boundary sliding dominates creep, that is, in the intermediate region of Fig. 18, can ordinarily sustain very large deformation before failure. This is the creep mechanism that leads to "superplastic" behavior in tension [21, 22, 23]. An extreme example is shown in Fig. 23. The joint in this figure is a fine-grained In-Bi-Sn eutectic solder crept in shear at intermediate strain rate.

In the classic eutectic microstructure the failure strain can be reduced by microstructural instabilities of the kind illustrated in Fig. 7. Particularly when the sample is tested in shear, inhomogeneities in the shear strain lead to the formation of thin, recrystallized bands in the plane of maximum shear. Since the material in these bands is relatively fine-grained, it creeps rapidly relative to the surrounding eutectic material. This mechanical inhomogeneity further concentrates the strain and leads to failure by cracking along the band, as illustrated in Fig. 24. The loss of elongation due to the formation of recrystallized bands is, however, mitigated by the fact that fine-grained material has a very high failure strain. Eutectic solders tested in shear often have large tertiary strains, despite local recrystallization. As illustrated in Fig. 16, even the Sn-Bi eutectic, which is one of the hardest of the low-melting-point solders, undergoes over 50% of its creep strain to failure at 20°C in the tertiary regime [16].

Stress relaxation

The strains developed during processing or during thermal excursions in service leave a solder joint in a stressed condition. The stress is then gradually relaxed by creep.[26,28] Neglecting primary creep, the rate of stress relaxation is governed by the steady-state creep rate. The residual stress in a joint strained in shear is

$$\tau = G\gamma \tag{2}$$

where G is the shear modulus and γ is the shear strain. Stress relaxation under steady-state conditions is, hence, governed by the differential equation

$$\frac{d\tau}{dt} = G\frac{d\gamma}{dt} = GA\tau^n \exp\left[-\frac{Q}{kT}\right] \tag{3}$$

The higher the strain rate at given stress, the higher the rate of stress relaxation.

It follows that it is desirable to use microstructurally soft solders, with relatively high creep rates, in applications where stress relaxation is desirable. This is often the case in optoelectronic devices that are used at essentially constant temperature, but must maintain close dimensional tolerances. The use of a soft solder makes it possible to relax residual stresses and establish alignment before the device is put into service.

Fatigue

Failure induced by thermal fatigue is one of the most important threats to the integrity of solder joints. The source of the fatigue load is the thermal cycle the joint experiences during service, as the device is turned on and off, or as the temperature of the environment changes. In many cases the strain cycle is predominantly in shear. In almost all cases the joint is cycled at a high homologous temperature, so the cyclic deformation that causes fatigue is largely creep. In a typical solder joint, the cyclic deformation is largely in shear, so the relevant behavior is creep fatigue in shear.

Creep fatigue is a difficult metallurgical problem, particularly in as-cast materials whose microstructures evolve as fatigue proceeds. But even without a detailed analysis of the phenomenon, it is possible to set out some general and useful guidelines regarding the role of microstructure on the fatigue process. The simple guiding principle is that the microstructure should resist the formation of the "persistent slip bands" that concentrate cyclic deformation and nucleate fatigue cracks. To accomplish this, one would like to homogenize the deformation as much as possible, and avoid the development of local stress concentrations within the material.

From this perspective, the classic eutectic microstructure is a particularly weak one, particularly when it is fatigued at a temperature above the recrystallization temperature of the material. As discussed above, and described in detail elsewhere [13, 24], inhomogenous shear leads to recrystallization and a locally soft microstructure. This concentrates shear deformation and promotes the early nucleation of fatigue cracks. The process is illustrated in Fig. 25, which illustrates the mechanism of isothermal fatigue failure in eutectic Pb-Sn. Similar behavior is observed in thermal fatigue [29], and in the service failures of eutectic solder joints [30].

To improve the fatigue resistance of eutectic solders it is desirable to break up the classic eutectic microstructure and homogenize the strain. There are at least three ways of doing this.

First, increasing the cooling rate during the solidification of the joint creates a more equiaxed microstructure and improves the fatigue life. Fig. 26 compares the rate of isothermal fatigue damage (as measured by the decrease in peak stress for a given strain cycle) for eutectic Pb-Sn solder joints prepare at three cooling rates (their microstructures are shown in Fig. 3). The slowly cooled material has a classic eutectic microstructure and fails rapidly. The fatigue life increases with the cooling rate. The quenched material has a fine-grained, equiaxed microstructure and a dramatically longer fatigue life. Fig. 27 shows the irregular profile of the fatigue crack in the fine-grained material.

Since high rates of cooling are easily and, usually, naturally achieved in small solder joints, it follows that small solder joints should have better fatigue resistance than more massive joints of the same nominal composition, and that every effort should be made to maximize the rate at which they are solidified. However, there are at least two other pertinent considerations. First, the maximum benefit of the fine-grained

microstructure is realized at relatively low strain rates, where superplastic deformation is possible. There is much less benefit to a fine grain size in joints that are, for whatever reason, cyclically deformed at high strain rates. Second, long service time at relatively high temperature will induce grain growth, and cause a gradual deterioration in the fatigue resistance.

Second, eutectic solder joints that cannot be quenched can be improved by adding chemical species that inhibit the formation of the classic eutectic microstructure. Prior work in this laboratory [5,6,15] has shown that small additions of In and Cd can be effective in improving the fatigue properties of eutectic Pb-Sn. The microstructural change associated with the In addition is illustrated in Fig. 4.

Third, the fatigue resistance of eutectic solder can be improved by shifting to a slightly off-eutectic composition that introduces islands of pro-eutectic material into the microstructure, as illustrated in Fig. 9. These islands homogenize deformation by providing ductile barriers to the formation of shear bands, as illustrated in Fig. 28 [15].

The same reasoning may be used to motivate the introduction of a distribution of a dispersed second phase into the solder to improve fatigue resistance. One of us suggested this method in earlier work [2]. This method may succeed if the second phase is ductile, but does not appear to work when the second phase is relatively hard. For example, the wetting of a Au-coated substrate by eutectic Pb-Sn introduces a dense dispersion of Au-Sn particles into the solder, as illustrated in Fig. 14. However, the fatigue resistance of the solder decreases significantly, as shown in Fig. 29 [35]. The reason is, apparently, a combination of the increase in creep strength (Fig. 21), and the possibility of local stress concentrations due to the hard inclusion particles.

CONCLUSION

The examples given above should suffice to show that the microstructure of a solder joint cannot be ignored if its mechanical properties are to be understood. Changes in the microstructure can, and do cause dramatic changes in mechanical properties and failure modes.

This fact has several implications for the design of reliable solder joints. First, the engineer should be cautious in his use of laboratory data to guide joint design. Unless the microstructures of the laboratory samples, and their microstructural evolution during testing, resemble those of the manufactured joints, the laboratory data may be misleading. In the case of eutectic solder joints, however, the fact that small, rapidly cooled solder joints usually have better mechanical properties than the bulk samples that are commonly used for laboratory testing may provide an added margin of safety. Second, analytic models that attempt to predict joint behavior should be viewed with some skepticism if they do not incorporate the effects of microstructure and microstructural evolution. Again, however, there is some margin of safety in even relatively crude empirical models when they are used to extrapolate service experience to new joint designs that are

microstructurally similar. Third, the nominal composition of the solder used in a joint is not sufficient to determine its microstructure or its mechanical properties. Not only are process and service conditions important, but small chemical changes from impurities or solder-substrate interactions can also have significant effects.

ACKNOWLEDGMENT

This work was funded by the Director, Office of Energy Research, Office of Basic Energy Sciences, Materials Sciences Division of the U.S. Department of Energy, under Contract NO. DE-AC03-76SF00098

REFERENCES

[1] Z. Mei, J. W. Morris, Jr., M. C. Shine, and T.S.E. Summers, *J. Electronic Mater.*, **20**, 599 (1991)

[2] J. W. Morris, Jr., and Z. Mei, Ch. 6 in *Solder Mechanics: A State of the Art Assessment*, D.R. Frear, W.B. Jones, K.R. Kinsman, Eds., TMS, Warrendale, PA, (1991)

[3] J. W. Morris, Jr., J. L. Freer Goldstein, and Z. Mei, Ch. 2 in *The Mechanics of Solder Alloy Interconnects*, S.N. Burchett, D.R. Frear, H.S. Morgan, and J.H. Lau, Eds., Van Nostrand Reinhold, New YORK, NY, (1993).

[4] Z. Mei and J. W. Morris, Jr., ASME *Journal of Electronic Packaging*, **114**, 104 (1992).

[5] L. K. Quan, M.S. Thesis University of California at Berkeley, August 1988.

[6] D. Tribula and J. W. Morris, Jr., ASME *Journal of Electronic Packaging*, **112**, 87 (1990).

[7] J.L.F. Goldstein, Ph.D. Thesis, University of California at Berkeley, Nov. 1993; and J. W. Morris, Jr., J. L. Freer Goldstein, and Z. Mei, JOM, **45**, 25 July 1993.

[8] J. W. Morris, Jr., D. Grivas, D. Tribula, T. Summers, and D. Frear, *Proc. 13th Naval Weapons Electronics Manuf.acturing Seminar,* China Lake, CA (1989)

[9] J.L.Freer Goldstein, and J. W. Morris, Jr., J. Electronic Mater. **23**, 477, (1994).

[10] Z. Mei and J. W. Morris, Jr., *J. Electronic Mater.*, **21**, 401 (1992) .

[11] Z. Mei, A. J. Sunwoo, and J. W. Morris, Jr., *Metall. Trans.* A, **23A**, 857 (1992)

[12] D. Grivas, D. Frear, L. Quan, and J. W. Morris, Jr., *J. Electronic Mater.*, **15**, 355 (1986).

[13] D. Tribula, Ph.D. Thesis, University of California at Berkeley, June 1990;

[14] J. Glazer, P. Kramer, and J. W. Morris, *Proc. Surface Mount International Conference*, San Jose, CA, August 1991; and P.A. Kramer, M.S. Thesis, University of California at Berkeley, May 1992.

[15] T.S.E. Summers, Ph.D. Thesis, University of California at Berkeley, May 1991; and ASME *Journal of Electronic Packaging*, **112**, 94 (1992).

[16] Z. Mei and J. W. Morris, Jr., *J. Electronic Mater.*, **21**, 599 (1992).

[17] J. E. Bird, A.J. Mukherjee, and J. F. Dorn, *Quantitative Relation Between Properties and Microstructure*, 255 (Israel University Press, 1969).

[18] D. Grivas, K. L. Murty, and J. W. Morris, Jr., *Acta Met*, **27**, 731 (1979).

[19] P.A. Kramer, J. Glazer, and J.W. Morris, Jr., *Metall. Trans.* A, **25A**, 1249, (1994)

[20] F. Bartels, H. Linch (Reynolds), P. Xu, and J. W. Morris, Jr., *Proc. Inter. Symp. Test ing and Failure Analysis*, (ISTFA), Los Angeles (1994).

[21] M. M. I. Ahmed, and T. G. Langdon, *Metall. Trans.* A, **8A**, 1832, (1977)

[22] R. S. Mishra, T. R. Bieler, and A. K. Mukherjee, *Scripta Met.*, **26**, 1605, (1992).

[23] G. J. Davies, J. W. Edington, C. P. Cutler, K. A. Padmayabhaum, *J. of Mat. Sci.*, **5**, 1091, (1970).

[24] D. Tribula and J. W. Morris, Jr., ASME *Journal of Electronic Packaging*, **111**, 83, (1989).

[25] D. Tribula, D. Grivas, D. R. Frear, and J. W. Morris, Jr., *Welding Research Supplement*, 404, October 1989.

[26] S. M. Lee, Ph.D. Thesis, University of Wisconsin at Madison, 1993.

[27] D. S. Stone, and M. M. Rashid, Ch. 4 in *The Mechanics of Solder Alloy Interconnects*, S.N. Burchett, D.R. Frear, H.S. Morgan, and J.H. Lau, Eds., Van Nostrand Reinhold, New YORK, NY, (1993).

[28] J. R. Wilcox, Ph. D. Thesis, Cornell University, 1990.

[29] D.R. Frear, D. Grivas, and J. W. Morris, Jr., JOM, **40**, 18, June 1988.

[30] R. Yenawine, M. Wolverton, A. Burkett, B. Waller, B. Russel, D. Spritz, *Proc. 11th Naval Weapons Electronics Manufacturing Seminar*, China Lake, CA (1987)

[31] H.S. Linch (Reynolds), M.S. Thesis, University of California at Berkeley, December 1993.

[32] H. L. Reynolds and J. W. Morris, Jr., *J. Electronic Mater.*, **24**, 1429 (1995).

[33] J. L. Freer Goldstein, and J. W. Morris, Jr., *Metall. Trans.* A, **25A**, 2715 (1994)

[34] F. Bartels, and J. W. Morris, Jr., unpublished work.

[35] P. A. Kramer, Z. Mei, and J. W. Morris, Jr., unpublished work.

[36] F. Bartels, H. L. Reynolds, and J. W. Morris, Jr., unpublished work.

FIGURE CAPTIONS

Figure 1: Sn-Pb phase diagram.

Figure 2: Optical micrograph showing the lamellar microstructure of a slow-cooled, Sn-Pb eutectic solder. Colonies and colony boundaries can be observed. [15]

Figure 3: Optical micrographs of Sn-Pb eutectic solder joints made with (a) furnace cooling, (b) air-cooling, and (c) quenching. [4]

Figure 4: Optical micrographs showing the effect of In additions on the microstructure of a 60Sn-40Pb solder joint. (a) 60Sn-40Pb, and (b) 58Sn-40Pb-2In. [5]

Figure 5: Optical micrographs showing microstructures of two eutectic In-Sn solder joints after solidification at relatively slow rates. (a) Cu substrate, and (b) Ni substrate. [7]

Figure 6: SEM micrograph showing Sn-Bi eutectic microstructure. The Sn-rich phase is decorated with Bi precipitates. [34]

Figure 7: Optical micrographs showing inhomogeneous shear bands developed in deformed (a) Pb-Sn eutectic [8] and (b) Bi-Sn eutectic[9] solder joints.

Figure 8: Optical micrograph showing Sn-depleted region at the interface between the Pb-Sn solder and the Cu-Sn intermetallic. [31]

Figure 9: Optical micrograph showing the microstructure of an off-eutectic Pb-Sn solder. [15]

Figure 10: Optical micrographs of 40Sn-40In-20Pb solder joint at (a) low and (b) high magnifications. [10]

Figure 11: SEM micrograph showing the composite nature of the Cu-Sn intermetallics which form when a Sn-rich solder and Cu substrate are used. [32]

Figure 12: SEM micrograph showing Cu_6Sn_5 intermetallics growing into Sn-Pb solder. [13]

Figure 13: Backscattered SEM image of In-Sn eutectic solder on Au-coated Cu plate, showing In_2Au intermetallic particles with a layer of undissolved Au underneath (bottom of micrograph). [3]

Figure 14: (a) Optical micrograph showing $AuSn_4$ intermetallics which form within eutectic Pb-Sn solder joints on Au-plated substrates. (b) Micrograph showing components of the microstructure. [14]

Figure 15: SEM micrographs of the surface of a pre-tinned sample after successively longer sputter times. Intermetallic particles can be seen protruding from the surface of the solder. [11]

Figure 16: Typical creep curve illustrating primary, steady-state, and tertiary regimes. [16]

Figure 17: Schematic showing creep behavior of fine-grained, eutectic Pb-Sn solder. [18]

Figure 18: Schematic illustrating the effect of grain (colony) size on the creep rate of eutectic Pb-Sn.

Figure 19: Creep behavior of Bi-Sn eutectic with "classic" (lamellar) microstructure. Different specimen geometries result in a range of cooling rates yet the microstructure and creep rate are nearly the same.

Figure 20: Creep behavior of In-Sn on (a) Cu and (b) Ni substrates.

Figure 21: Creep behavior of Pb-Sn eutectic solder containing 0, 0.2 and 1.0 wt.% Au at 65°C. [19]

Figure 22: Correlation between creep data and stress-strain data at 25°C. Creep data are plotted as steady-state strain rate vs. applied shear stress and stress-strain data are plotted as strain rate vs. peak shear stress. [20]

Figure 23: Micrograph of a fine-grained In-Bi-Sn solder joint after approximately 200% shear strain. [34]

Figure 24: Micrograph showing crack which develops along coarsened band of Pb-Sn joint tested in creep. [24]

Figure 25: Micrograph showing isothermal fatigue failure in a eutectic Pb-Sn joint. [25]

Figure 26: Plots of peak load vs. cycle in strain-controlled fatigue tests at (a) 65 °C and (b) 20 °C of solder joints solidified at different cooling rates: quenched(Q), air-cooled(AC), and furnace-cooled(FC). [4]

Figure 27: Optical micrograph of a quenched Pb-Sn solder joint after fatigue testing. [4]

Figure 28: Micrograph of off-eutectic Pb-Sn solder joint after fatigue testing. Crack propagation appears to terminate at "island" of pro-eutectic Pb-phase. [15]

Figure 29: Plot showing decrease in fatigue resistance for Pb-Sn eutectic solder joints with increase in Au concentration. [35]

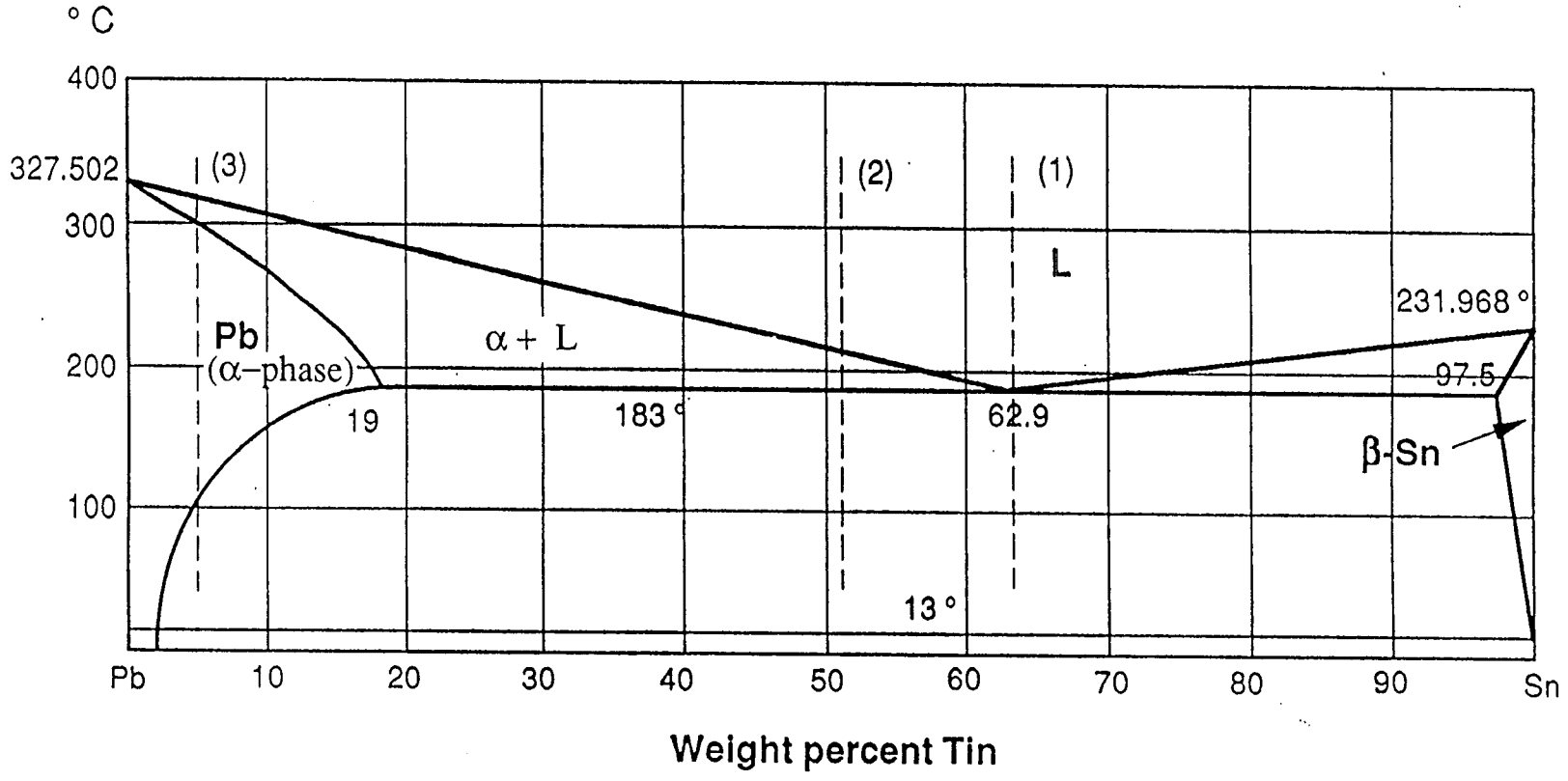

Figure 1: Sn-Pb phase diagram.

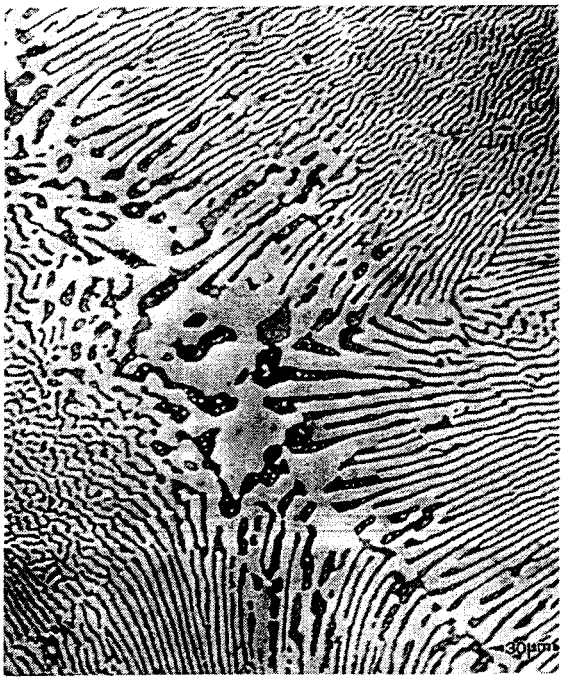

Figure 2: Optical micrograph showing the lamellar microstructure of a slow-cooled, Sn-Pb eutectic solder. Colonies and colony boundaries can be observed. [15]

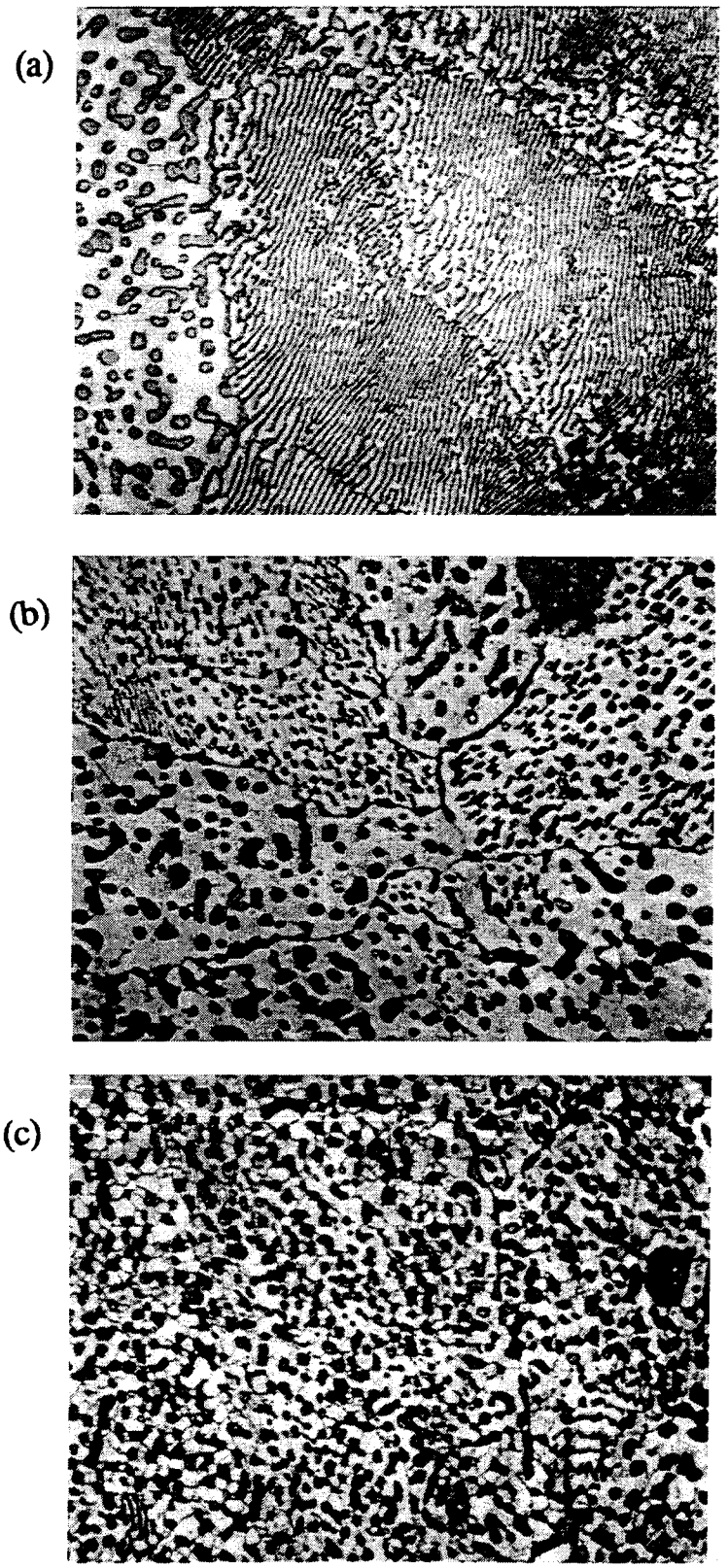

Figure 3: Optical micrographs of Sn-Pb eutectic solder joints made with (a) furnace cooling, (b) air-cooling, and (c) quenching. [4]

(a)

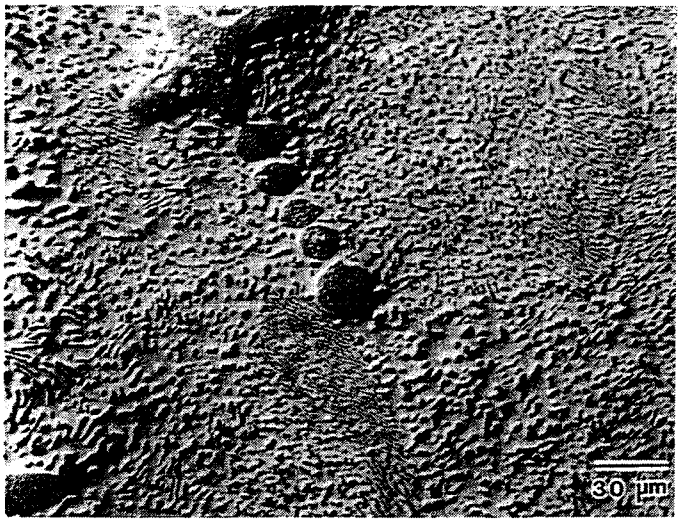

(b)

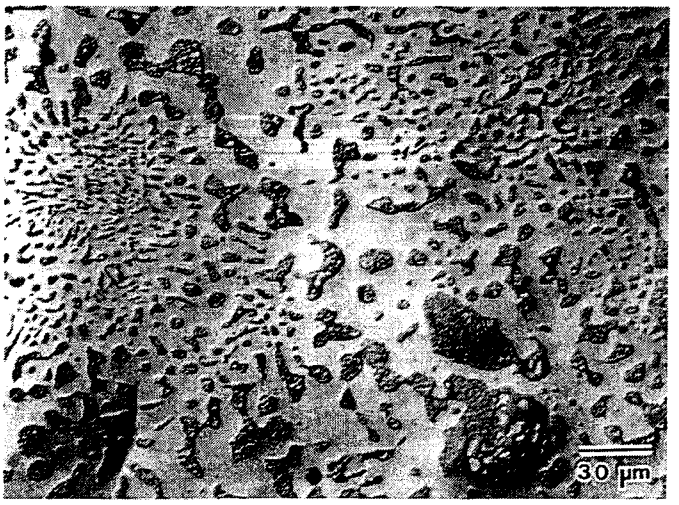

Figure 4: Optical micrographs showing the effect of In additions on the microstructure of a 60Sn-40Pb solder joint. (a) 60Sn-40Pb, and (b) 58Sn-40Pb-2In. [5]

(a)

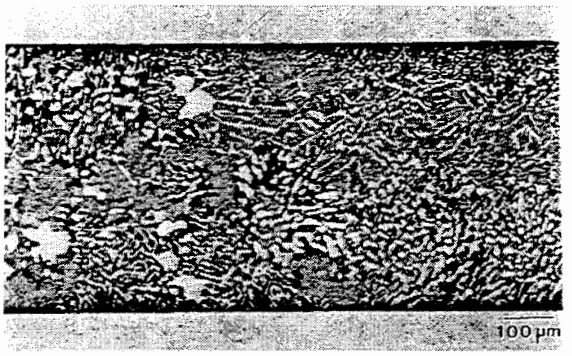

(b)

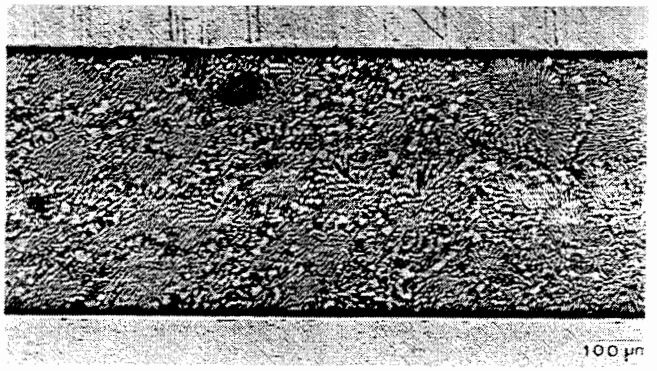

Figure 5: Optical micrographs showing microstructures of two eutectic In-Sn solder joints after solidification at relatively slow rates. (a) Cu substrate, and (b) Ni substrate. [7]

Figure 6: SEM micrograph showing Sn-Bi eutectic microstructure. The Sn-rich phase is decorated with Bi precipitates. [34]

(a)

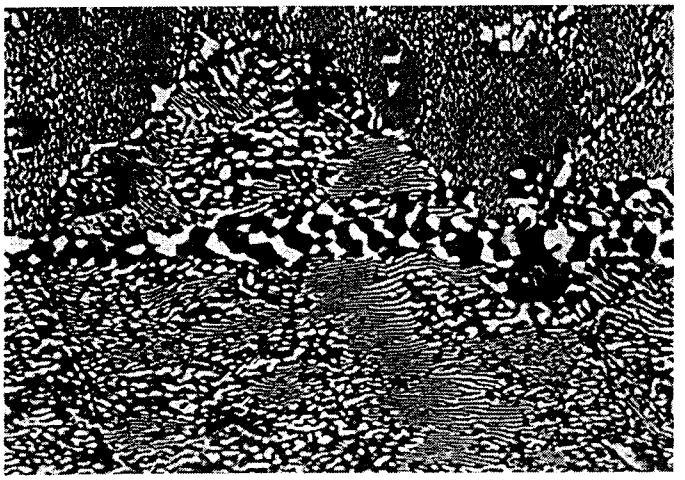

(b)

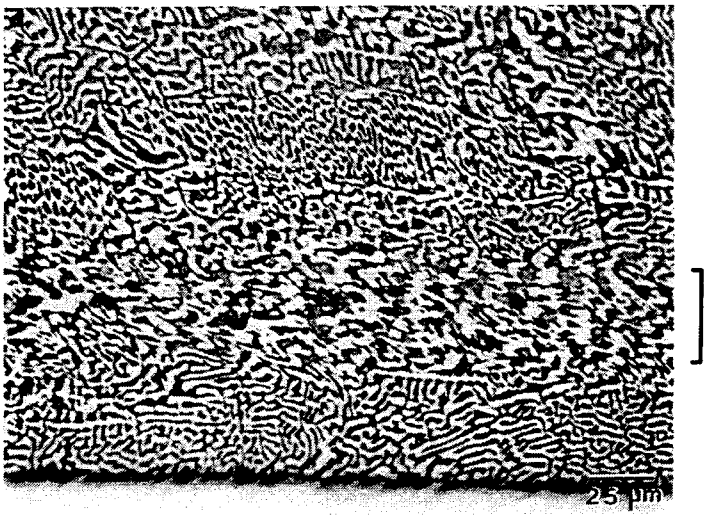

Figure 7: Optical micrographs showing inhomogeneous shear bands developed in deformed (a) Pb-Sn eutectic [8] and (b) Bi-Sn eutectic[9] solder joints.

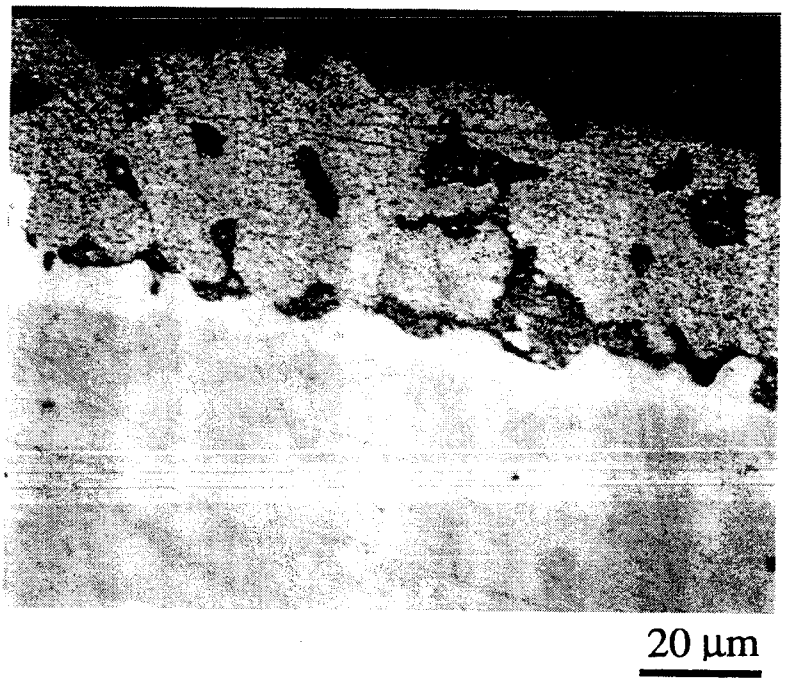

Figure 8: Optical micrograph showing Sn-depleted region at the interface between the Pb-Sn solder and the Cu-Sn intermetallic. [31]

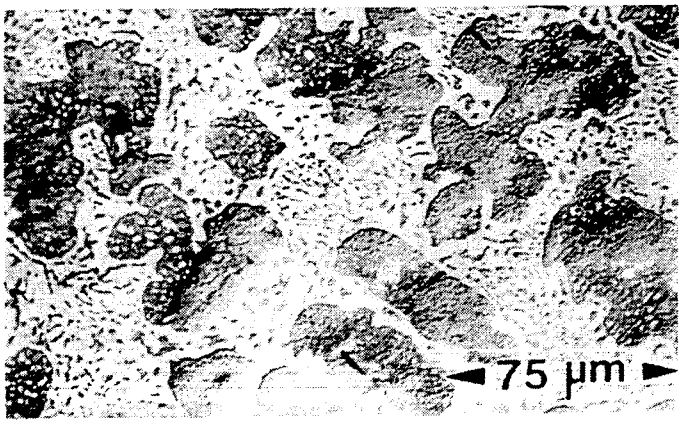

Figure 9: Optical micrograph showing the microstructure of an off-eutectic Pb-Sn solder. [15]

(a)

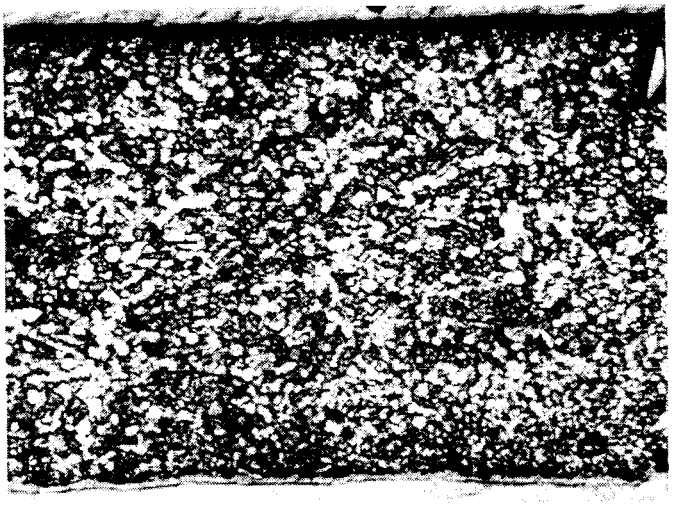

25 μm

(b)

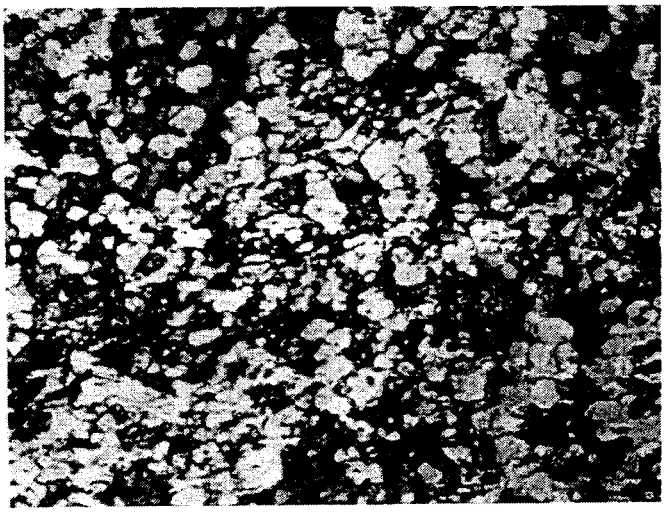

10 μm

Figure 10: Optical micrographs of 40Sn-40In-20Pb solder joint at (a) low and (b) high magnifications. [10]

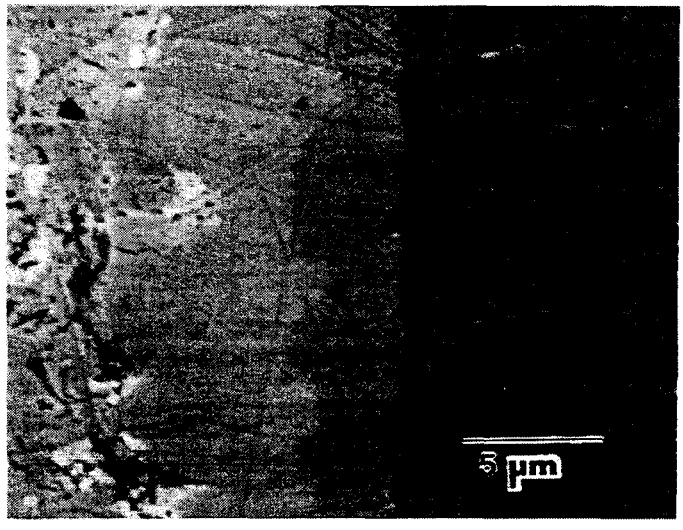

Figure 11: SEM micrograph showing the composite nature of the Cu-Sn intermetallics which form when a Sn-rich solder and Cu substrate are used. [32]

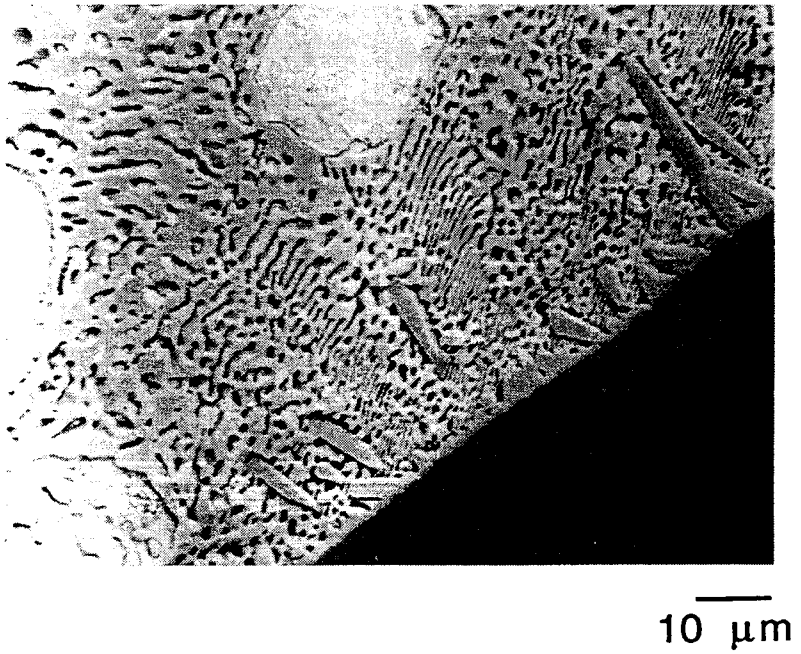

Figure 12: SEM micrograph showing Cu_6Sn_5 intermetallics growing into Sn-Pb solder. [13]

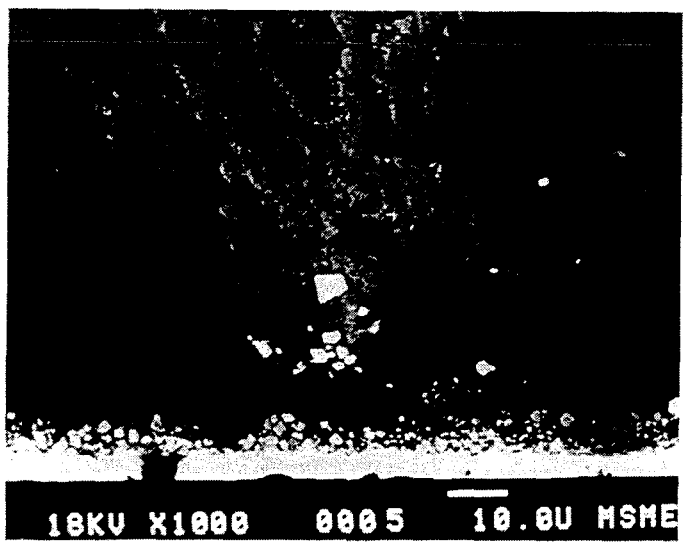

Figure 13: Backscattered SEM image of In-Sn eutectic solder on Au-coated Cu plate, showing In_2Au intermetallic particles with a layer of undissolved Au underneath (bottom of micrograph). [3]

(a)

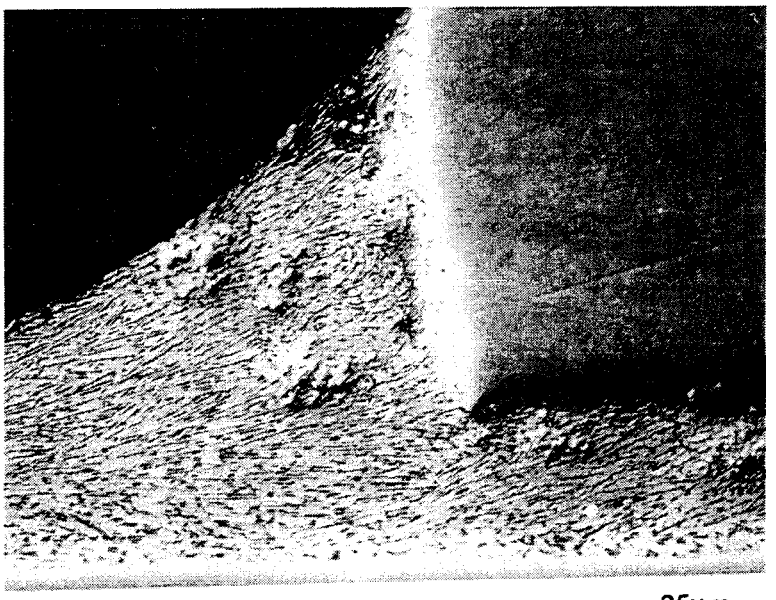

(b)

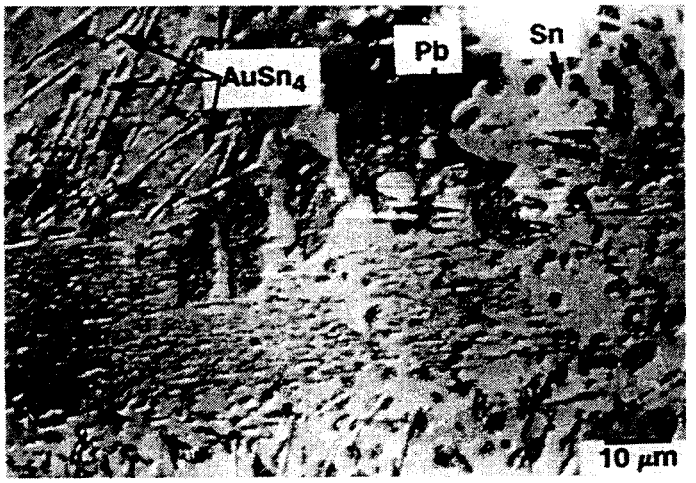

Figure 14: (a) Optical micrograph showing $AuSn_4$ intermetallics which form within eutectic Pb-Sn solder joints on Au-plated substrates. (b) Micrograph showing components of the microstructure. [14]

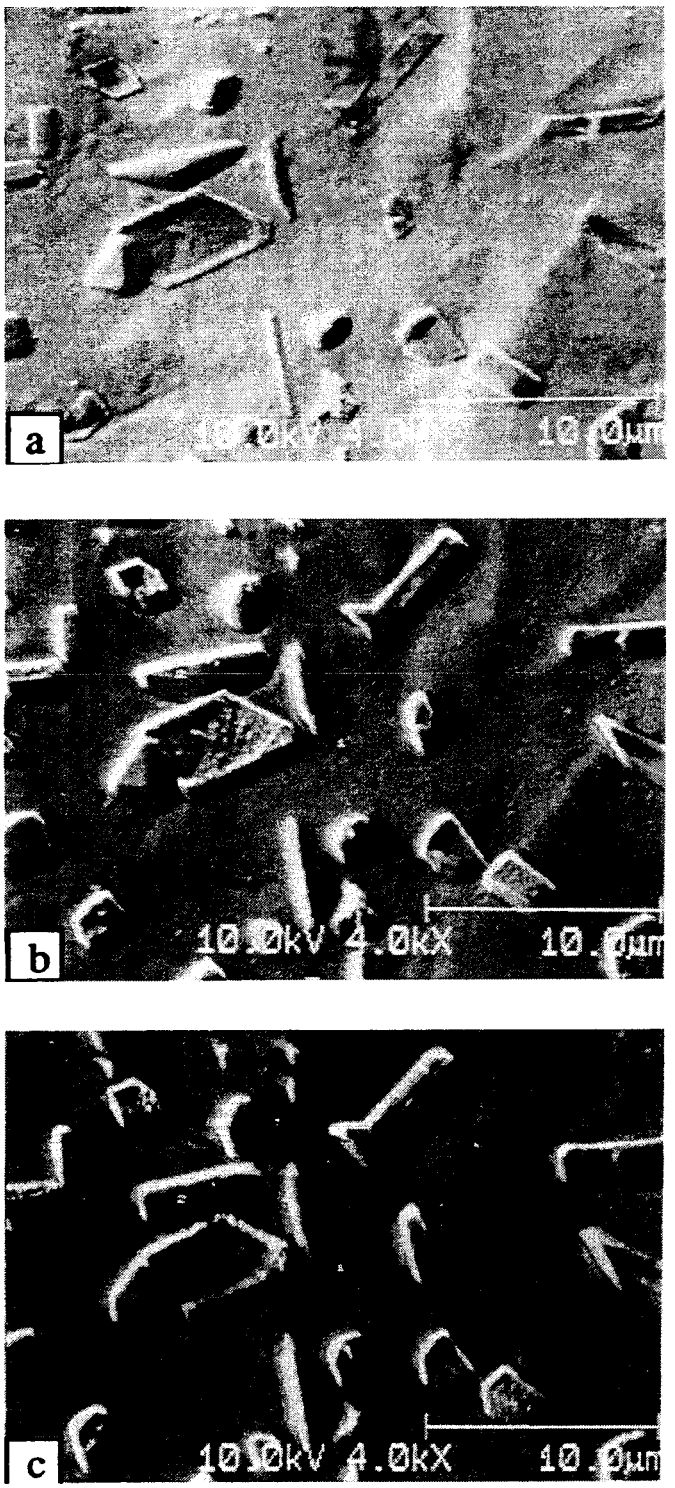

Figure 15: SEM micrographs of the surface of a pre-tinned sample after successively longer sputter times. Intermetallic particles can be seen protruding from the surface of the solder. [11]

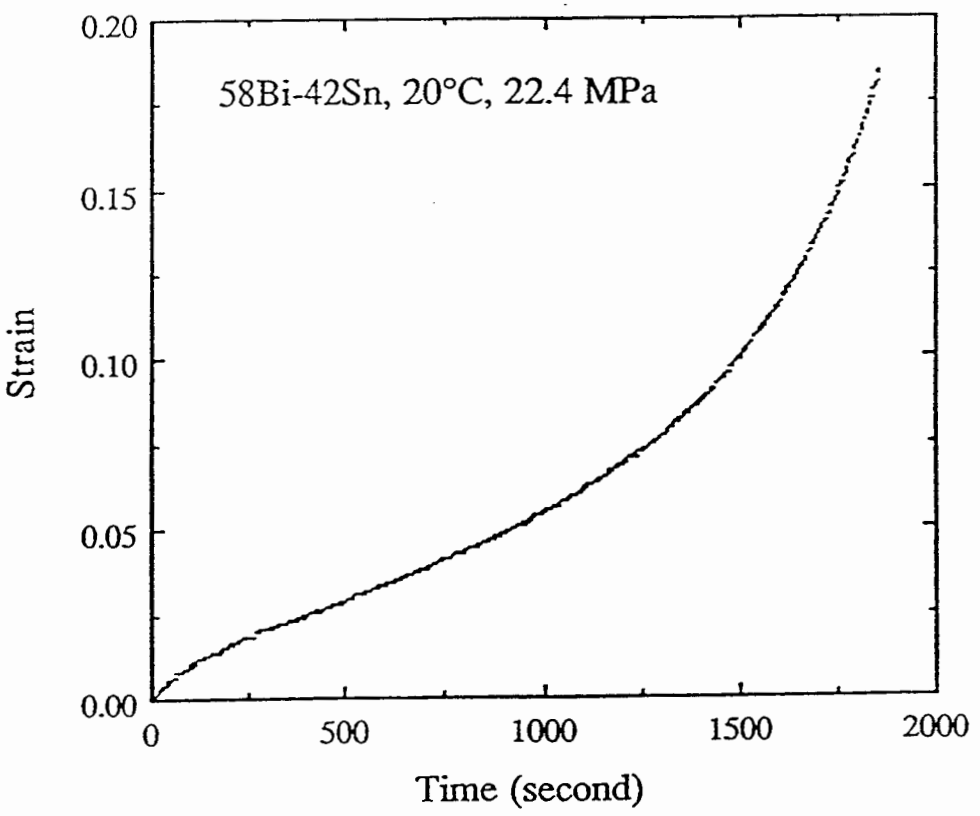

Figure 16: Typical creep curve illustrating primary, steady-state, and tertiary regimes. [16]

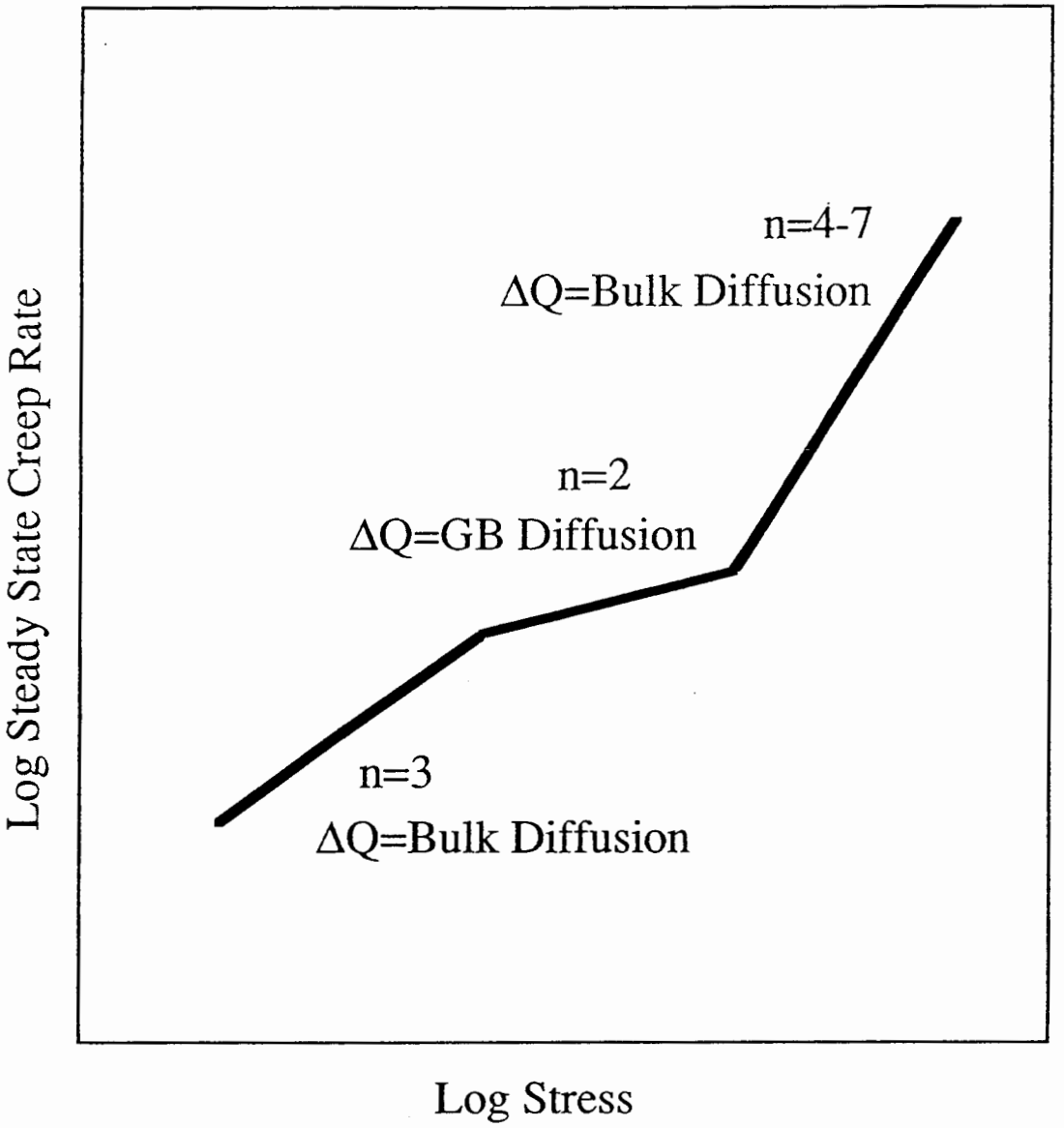

Figure 17: Schematic showing creep behavior of fine-grained, eutectic Pb-Sn solder. [18]

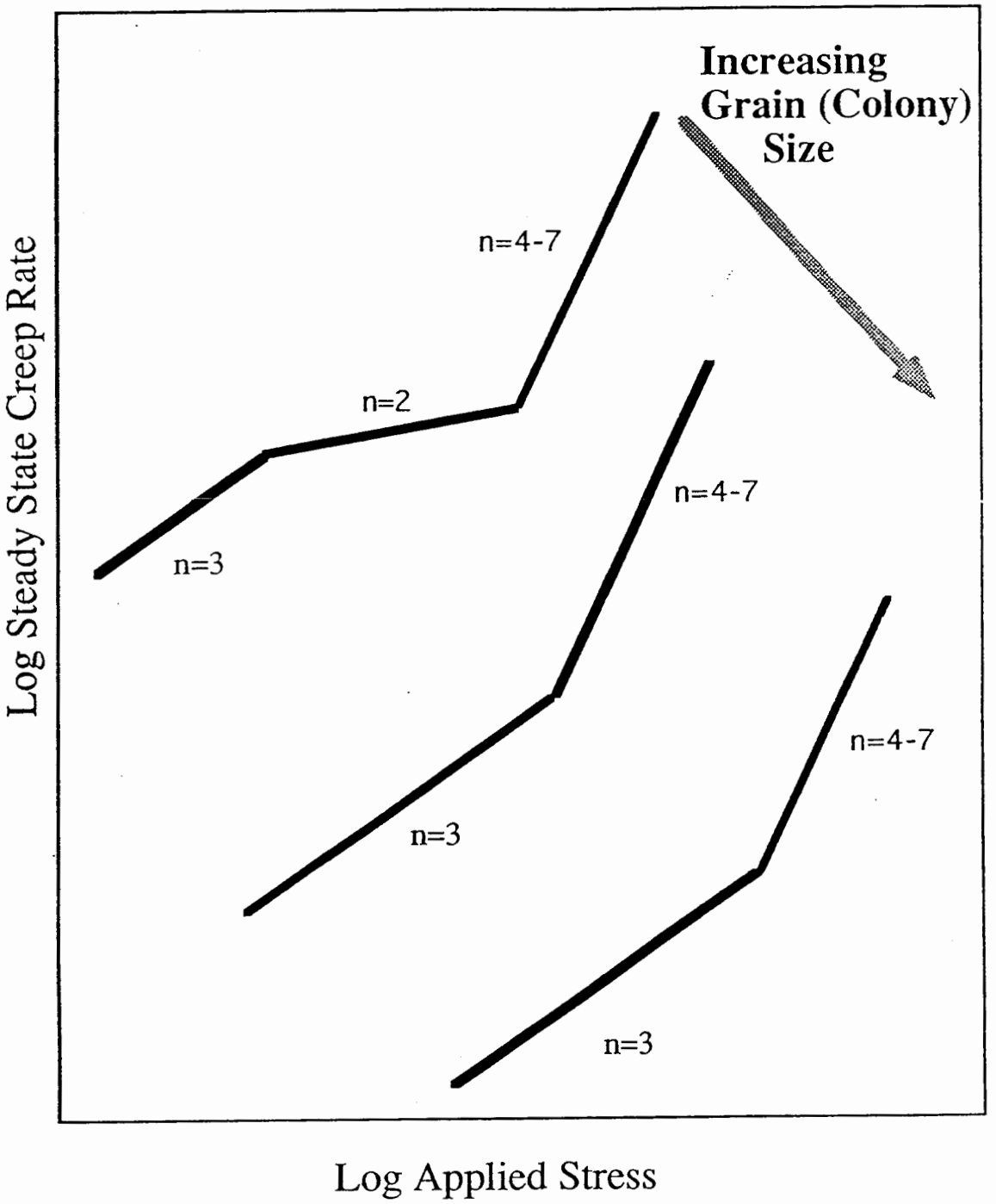

Figure 18: Schematic illustrating the effect of grain (colony) size on the creep rate of eutectic Pb-Sn.

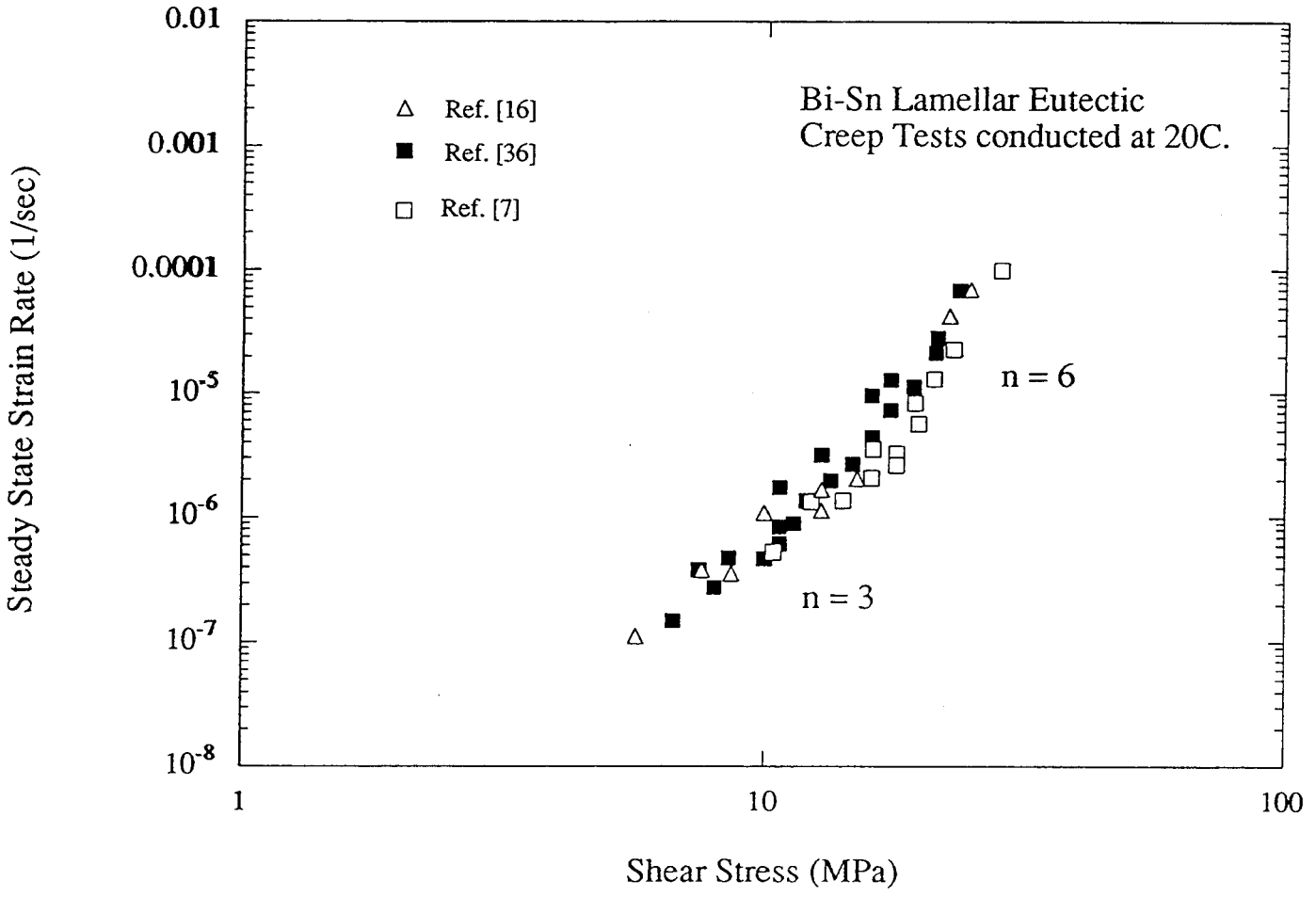

Figure 19: Creep behavior of Bi-Sn eutectic with "classic" (lamellar) microstructure. Different specimen geometries result in a range of cooling rates yet the microstructure and creep rate are nearly the same.

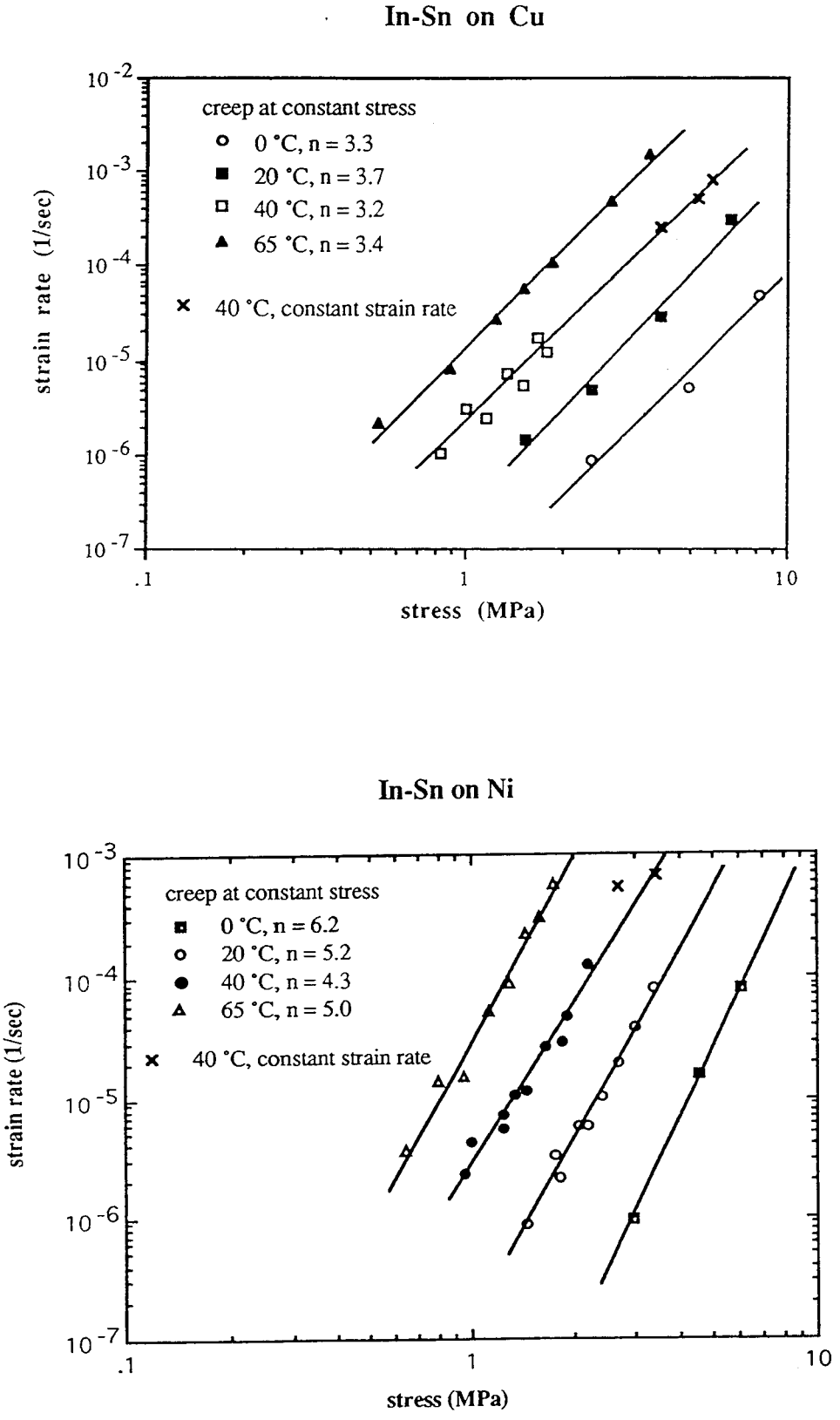

Figure 20: Creep behavior of In-Sn on (a) Cu and (b) Ni substrates.

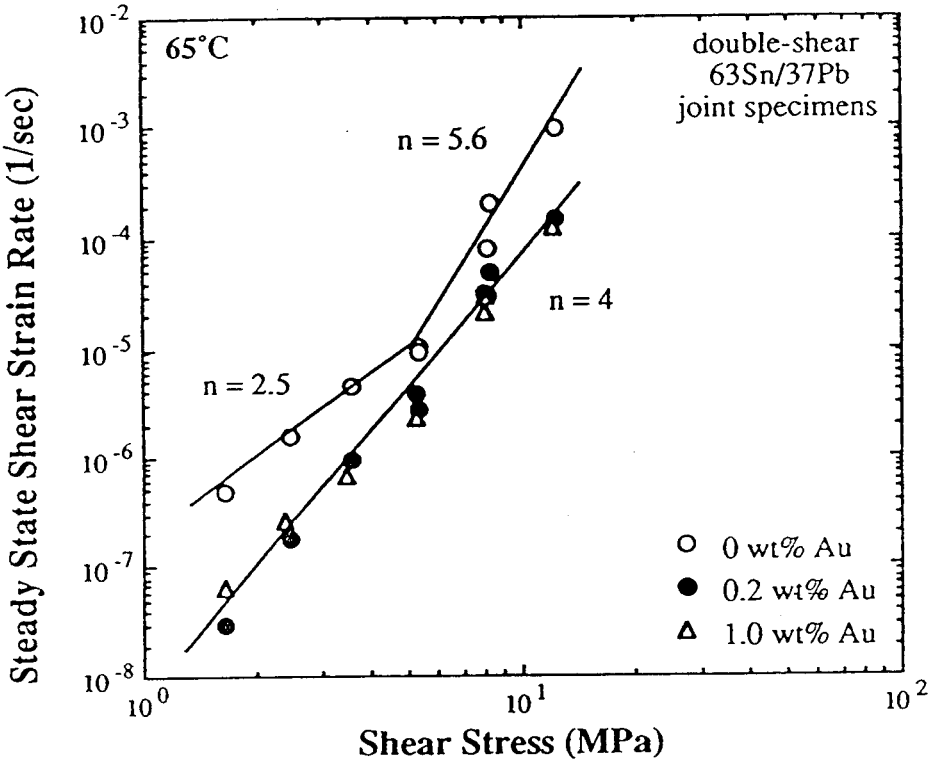

Figure 21: Creep behavior of Pb-Sn eutectic solder containing 0, 0.2 and 1.0 wt.% Au at 65°C. [19]

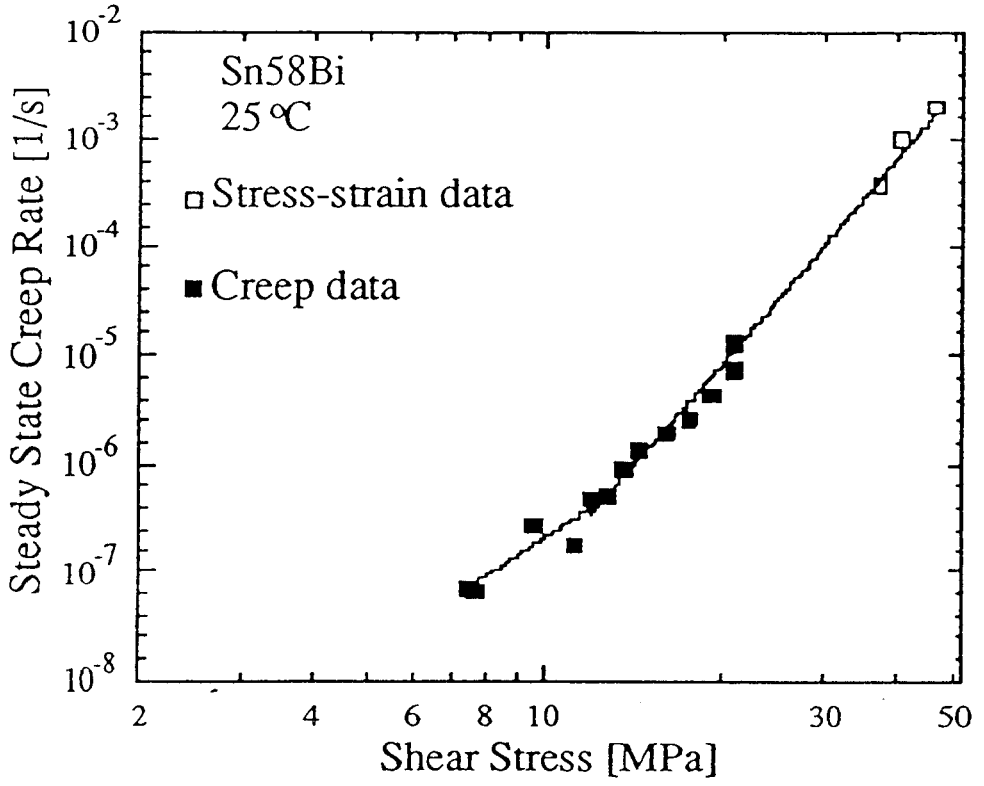

Figure 22: Correlation between creep data and stress-strain data at 25°C. Creep data are plotted as steady-state strain rate vs. applied shear stress and stress-strain data are plotted as strain rate vs. peak shear stress. [20]

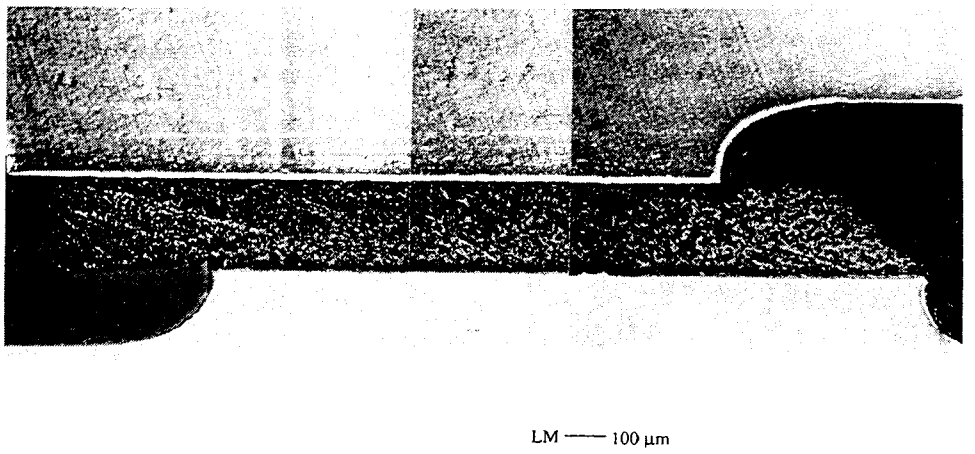

Figure 23: Micrograph of a fine-grained In-Bi-Sn solder joint after approximately 200% shear strain. [34]

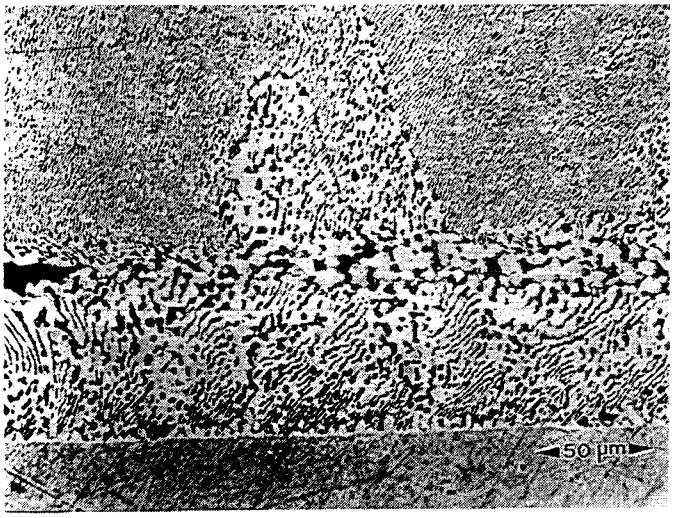

Figure 24: Micrograph showing crack which develops along coarsened band of Pb-Sn joint tested in creep. [24]

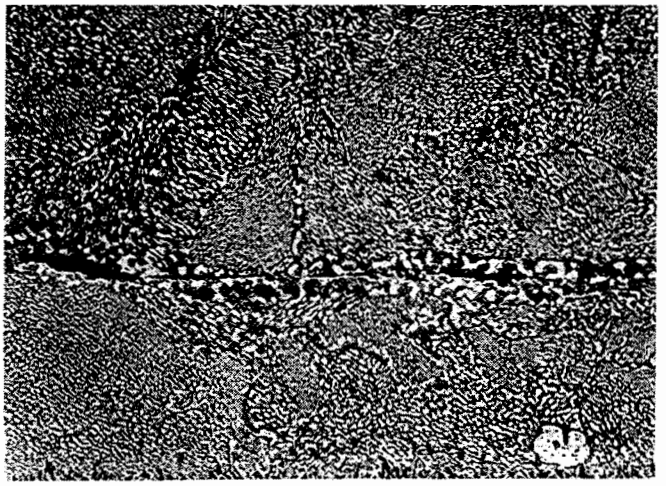

Figure 25: Micrograph showing isothermal fatigue failure in a eutectic Pb-Sn joint. [25]

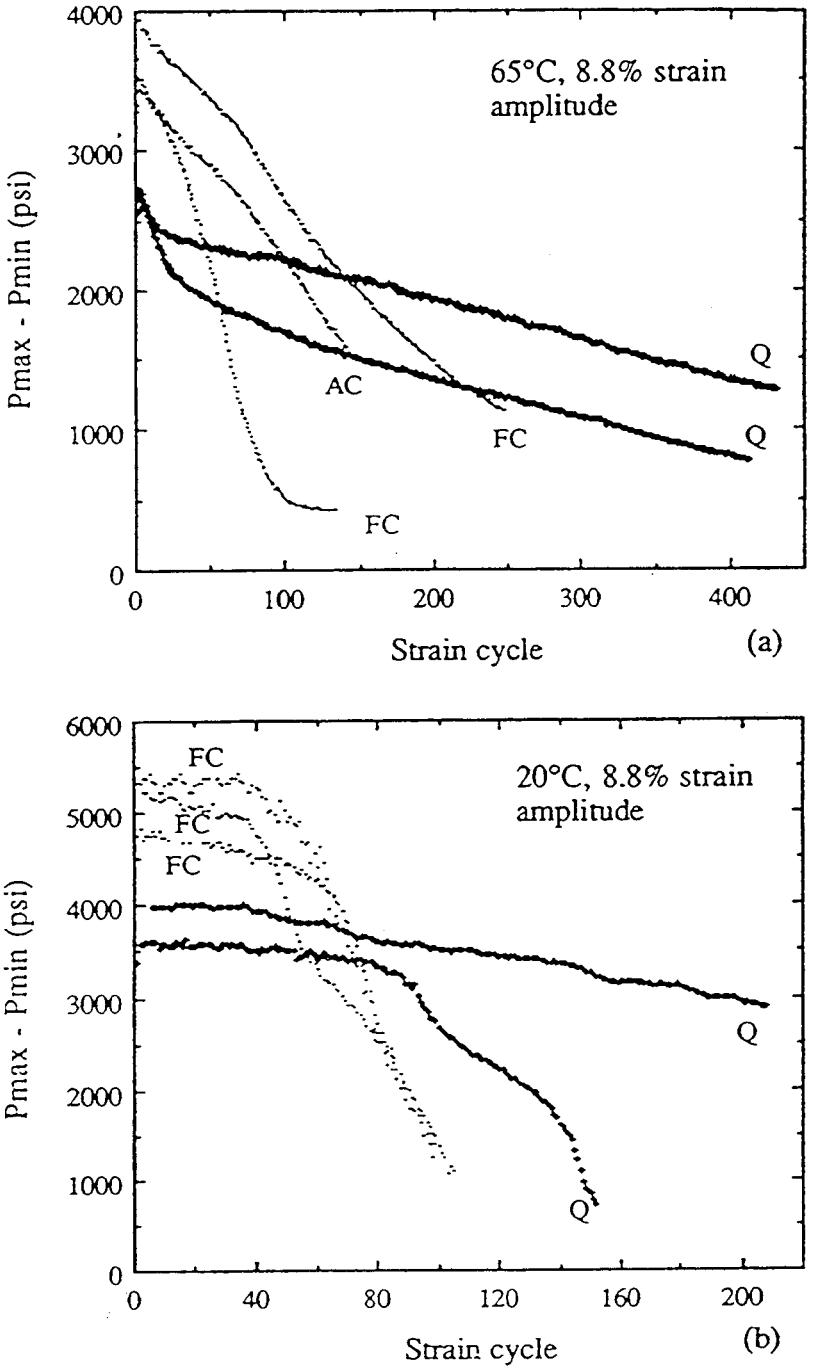

Figure 26: Plots of peak load vs. cycle in strain-controlled fatigue tests at (a) 65 °C and (b) 20 °C of solder joints solidified at different cooling rates: quenched(Q), air-cooled(AC), and furnace-cooled(FC). [4]

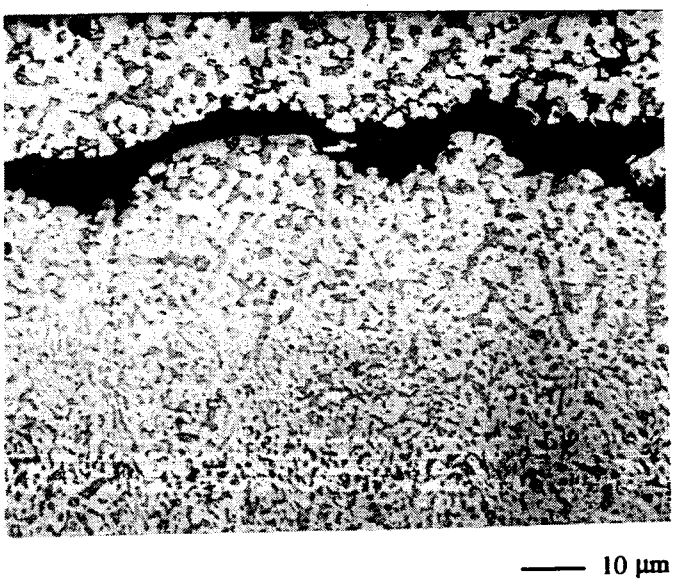

Figure 27: Optical micrograph of a quenched Pb-Sn solder joint after fatigue testing. [4]